Effect of Clay Addition on the Morphology and Thermal Behavior of Polyamide 6

Ting-Cheng Li,[1,2] Jianhua Ma,[3] Min Wang,[2] Wuiwui Chauhari Tjiu,[4] Tianxi Liu,[1] Wei Huang[2]

[1]*Key Laboratory of Molecular Engineering of Polymers of Chinese Ministry of Education, Department of Macromolecular Science, Fudan University, Shanghai 200433, People's Republic of China*
[2]*Laboratory of Advanced Materials, Fudan University, Shanghai 200433, People's Republic of China*
[3]*Department of Chemical Engineering, Chengde Petroleum College, Chengde 067000, People's Republic of China*
[4]*Institute of Materials Research and Engineering, 3 Research Link, Singapore 117602*

Received 13 June 2005; accepted 9 January 2006
DOI 10.1002/app.25378
Published online in Wiley InterScience (www.interscience.wiley.com).

ABSTRACT: The nanostructure, morphology, and thermal properties of polyamide 6 (PA6)/clay nanocomposites were studied with X-ray scattering, differential scanning calorimetry (DSC), and transmission electron microscopy (TEM). The wide-angle X-ray diffraction (WAXD) and TEM results indicate that the nanoclay platelets were exfoliated throughout the PA6 matrix. The crystallization behavior of PA6 was significantly influenced by the addition of clay to the polymer matrix. A clay-induced crystal transformation from the α phase to the γ phase for PA6 was confirmed by WAXD and DSC; that is, the formation of γ-form crystals was strongly enhanced by the presence of clay. With various clay concentrations, the degree of crystallinity and crystalline morphology (e.g., spherulite size, lamellar thickness, and long period) of PA6 and the nanocomposites changed dramatically, as evidenced by TEM and small-angle X-ray scattering results. The thermal behavior of the nanocomposites was investigated with DSC and compared with that of neat PA6. The possible origins of a new clay-induced endothermic peak at high temperature are discussed, and a model is proposed to explain the complex melting behavior of the PA6/clay nanocomposites. © 2006 Wiley Periodicals, Inc. J Appl Polym Sci 103: 1191–1199, 2007

Key words: clay; morphology; nanocomposites; polyamides; thermal properties

INTRODUCTION

Compounding polymers with inorganic materials has long been an interesting topic of scientific research and industrial applications because inorganic materials can be used to improve the mechanical and barrier properties and high-temperature durability and to reduce the flammability of resultant polymer composites.[1,2] Among various inorganic fillers, fibers and anisotropic particles with large aspect ratios (length/diameter ratios), such as mica-type clay or layered silicates (e.g., montmorillonite, hectorite, and saponite), have proven to be particularly effective in polymer matrix reinforcement.[3] Usually, the dispersion of clay particles in a polymer matrix can result in the formation of three types of composite materials.[1] The first type is conventional phase-separated composites, in which the clay and the polymer host remain immiscible; this results in poor mechanical properties of the composite material. The second type is intercalated polymer–clay nanocomposites, which are formed by the insertion of one or more molecular chains of the polymer into the interlayer or gallery space. The last type is exfoliated or delaminated polymer–clay nanocomposites, which are formed when the clay nanolayers are individually dispersed in the continuous polymer matrix. Exfoliated polymer–clay nanocomposites are especially desirable for improved properties because the large aspect ratio and homogeneous dispersion of clay result in a huge interfacial area between the polymer and clay.[4]

Among polymer/clay nanocomposites, polyamide 6 (PA6) based clay nanocomposites were the first studied systems; the study of these systems was pioneered by Toyota research group in 1993.[2,5–7] Since then, many investigations have been made on the preparation procedure, mechanical properties,[3,8,9] effect of the addition of clay on the crystalline structures and morphologies,[10–14] thermal degradation,[15] and rheological properties of PA6.[16] It is known that the presence of modified particles (e.g., rubber/inorganic filler particles) directly influences the morphology, crystallization behavior, and consequently, melting behavior of the thermoplastic polymer matrix. Although intensive research efforts have recently been devoted to the effect of clay addition on the crystallization behavior of the PA6 matrix,[17–19] to our knowledge, the effect of clay on the morphologies and especially the melting behavior of PA6 has not been

Correspondence to: T. X. Liu (txliu@fudan.edu.cn).

Journal of Applied Polymer Science, Vol. 103, 1191–1199 (2007)

well identified. These issues are systematically addressed in this article with X-ray scattering, microscopy, and thermal analysis results. The correlation between the concentration of clay and the structure and the thermal properties of the nanocomposites were also investigated.

EXPERIMENTAL

Materials and sample preparation

The PA6 pellets (grade SF1080A) used in this study were products of Ube Industries (Yamaguchi, Japan) under license from Toyota. The unmodified pristine clay and modified organoclay (Nanomer I.30TC) were supplied by Nanocor, Inc. (Arlington Heights, IL) All of the samples were dried in a vacuum oven at 80°C for 24 h before mixing. A wide range of PA6/clay nanocomposites containing 0, 2.5, 5, 7.5, and 10 wt % organoclay were prepared via a melt-compounding method with a Brabender (Duisburg, Germany) twin-screw extruder at 250°C with a screw speed of 80 rpm. The extruded pellets were dried at 90°C for at least 12 h in a vacuum oven to remove the absorbed water due to the high moisture absorption capability of polyamides. The as-prepared nanocomposite samples were used for subsequent X-ray scattering and thermal analysis measurements.

Characterization

Wide-angle X-ray diffraction (WAXD) was performed with a Philips (Almelo, The Netherlands) analytical X-ray (X'Pert) with nickel-filtered Cu $K\alpha_1$ radiation source ($\lambda = 0.1542$ nm) under a voltage of 45 kV and a current of 40 mA. The WAXD patterns were recorded with a step size of 0.05° from $2\theta = 2$ to 30°.

Small-angle X-ray scattering (SAXS) experiments were performed on a small-angle diffractometer (Bruker Nanostar (Karlsruhe, Germany)), with a Cu $K\alpha_1$ radiation source ($\lambda = 0.1542$ nm). The SAXS data were corrected for absorption, background scattering, and fluctuation of the incident beam intensity; the data were then smoothed with procedures described previously.[20] The one-dimensional correlation function was calculated with the approach developed by Strobl and coworkers.[21,22] The long period (L) was obtained from the maximum peak of the corrected Lorentz curves with the Bragg law. The lamellar thickness (l_c) was estimated with the following equation:

$$l_c = L \times W_c$$

where W_c is the degree of crystallinity, which could be obtained by calorimetry or X-ray scattering.[23]

The morphology of the PA6/clay nanocomposites was studied with a Philips CM300-FEG transmission electron microscope under an acceleration voltage of 200 kV. Thin sections of the nanocomposites (thickness $\approx$ 70 nm) for transmission electron microscopy (TEM) observations were cut from injection-molded bars under cryogenic conditions with a Leica (Wetzlar, Germany) ultramicrotome equipped with a diamond knife. For the observation of clay morphology, no selective staining was required due to a large difference in electron density between the clay and polymer matrix. To identify the lamellar morphology of PA6 obscured by clay addition, however, the thin sections were stained by OsO_4 for contrast enhancement.

Differential scanning calorimetry (DSC) experiments were performed in a TA DSC-2920 (TA Instruments, New Castle, DE), coupled with a TA-2000 control system. The samples were heated or cooled at a scanning rate of 10°C/min under a nitrogen atmosphere to minimize oxidation. To study of the effect of annealing temperature (T) on the melting behavior of PA6 and the PA6/clay nanocomposites, the samples were isothermally melt-crystallized at different temperatures for 6 h before subsequent heating in DSC. DSC curves were also recorded at different scanning rates to investigate the effect of heating rate on the thermal properties of PA6 and the nanocomposites.

RESULTS AND DISCUSSION

WAXD and TEM study of the nanostructure of clay in the PA6 matrix

The WAXD patterns for the pristine (natural) clay, organically modified clay (organoclay), neat PA6, and nanocomposite with 2.5 wt % clay as an example are illustrated in Figure 1. The WAXD pattern of the natural clay exhibited a diffraction peak around $2\theta = 6.9°$, which corresponded to a basal spacing of 1.42 nm. For the organoclay, the diffraction peak of the basal plane shifted to $2\theta = 4.1°$ with a d-spacing of 2.39 nm, which indicated that a periodic and swollen intercalated structure was formed when the surfactant was inserted into the host gallery of the clay platelets. For neat PA6, two main diffraction peaks were observed at about $2\theta = 20$ and 23.7°, which were attributed to the α(100) and α(002/202) crystal planes, respectively.[19,24–26] After the organoclay with PA6 was incorporated by melt compounding, the basal-plane diffraction peak of the organoclay disappeared in the WAXD patterns, which clearly indicated the formation of an exfoliated nanostructure, in view of the definition of exfoliation generally adopted in the literature.[27]

The previous WAXD results were further confirmed by TEM observation (Fig. 2). The separated dark lines (clay platelets) were homogeneously distributed in the polymer matrix for the PA6/clay (97.5/2.5) system. No clear intercalated morphology and aggre-

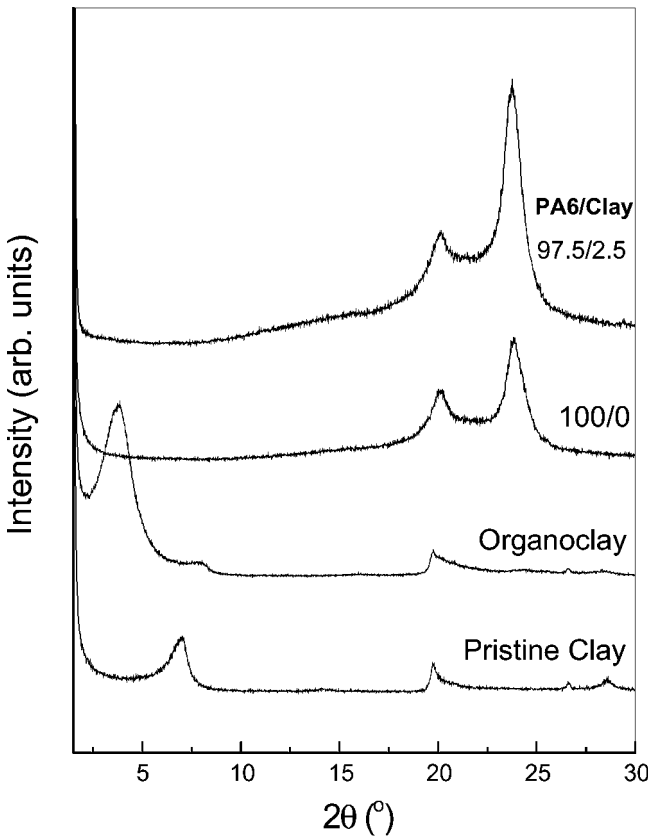

Figure 1 WAXD patterns of the pristine clay, organoclay, neat PA6, and PA6/clay nanocomposite sample with 2.5 wt % organoclay.

gated clay particles were detected. However, the presence of an intercalated clay structure could not be fully excluded, as both morphologies usually coexist among all polymer/clay systems.[23] The relative proportion of intercalated and exfoliated species increased with increasing nanoclay content.[28] It has been documented that the exfoliated structure is the dominant population when the clay concentration is low (e.g., $\leq$ 5 wt %), whereas above that, a mixture of intercalated and exfoliated structures is usually formed.[29] As shown in Figure 2, a processing-induced clay orientation was also observed.

DSC and WAXD study of the polymorphism and crystallinity of PA6 and the PA6/clay nanocomposites

Figure 3 shows the DSC heating curves of neat PA6 and the nanocomposites as a function of clay concentration. For clarity, some of the DSC curves shown here were shifted vertically. For neat PA6, on heating, only one endothermic peak ($T_{m,\alpha}$), which was associated with the melting of α-form crystals of PA6, was observed at 225°C;[17,19,30] this indicated that in the neat PA6 specimen, the α crystals were the dominant crystalline phase. By incorporation with clay, another

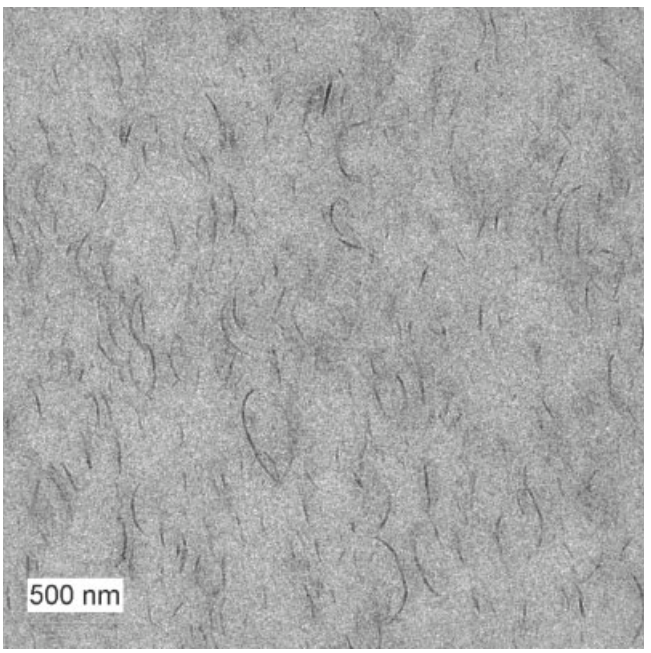

Figure 2 TEM image showing an exfoliated clay morphology in the nanocomposite sample with 2.5 wt % clay.

endothermic peak ($T_{m,\gamma}$), which corresponded to the melting of the less stable γ-form crystals of PA6, was observed at around 215°C as a shoulder of $T_{m,\alpha}$.[17,19,30]

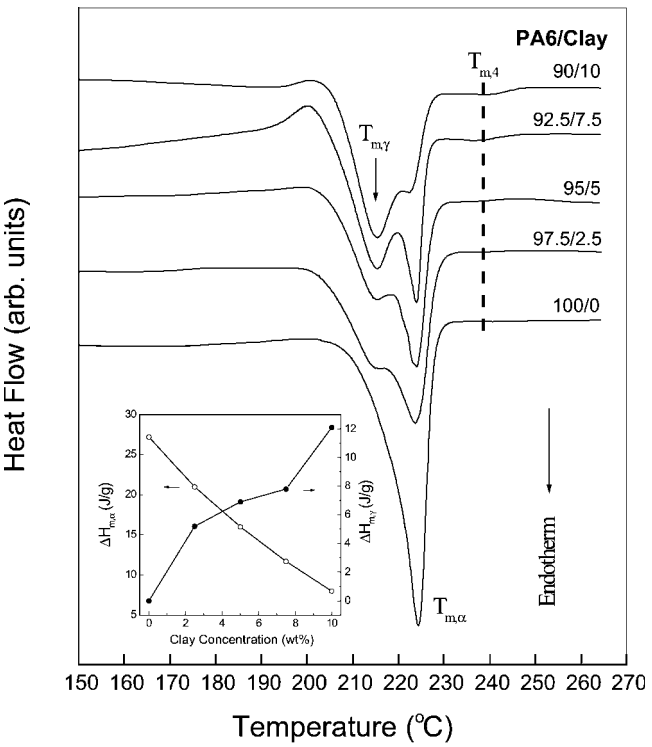

Figure 3 DSC heating curves for neat PA6 and the nanocomposite samples. The insert shows the enthalpies of the melting peaks of both the α and γ crystals ($\Delta H_{m,\alpha}$ and $\Delta H_{m,\gamma}$, respectively) as a function of clay concentration (heating rate = 10°C/min).

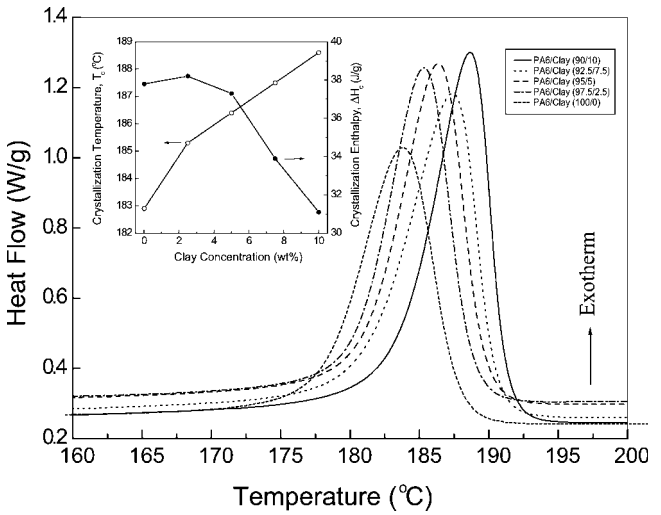

Figure 4 DSC cooling curves for neat PA6 and the nanocomposite samples. The insert shows the T_c values and the enthalpies of the crystallization peaks (ΔH_c's) as a function of clay concentration (cooling rate = 10°C/min).

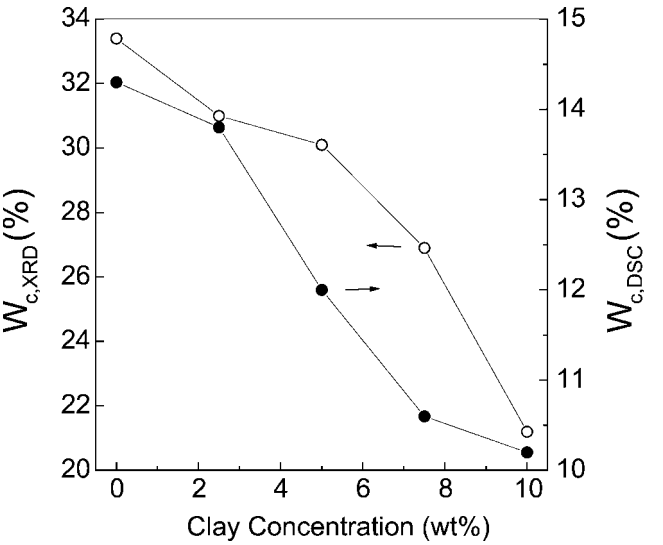

Figure 6 W_c as a function of clay loading, as estimated by WAXD and DSC measurements.

With increasing clay content, the magnitude of $T_{m,\gamma}$ was greatly enhanced, whereas the magnitude of $T_{m,\alpha}$ gradually decreased (as shown in the insert in Fig. 3). Nevertheless, their positions remained almost unchanged. Clearly, clay addition promoted the $\alpha \rightarrow \gamma$ crystal-phase transformation (this was further supported by the WAXD results, as shown later). Interestingly, on the heating curves, a new but very weak endothermic peak ($T_{m,4}$) was detected at about 237°C (as indicated by the dashed line in Fig. 3) for the nanocomposites. The possible origins of this abnormal melting peak are discussed later.

On the cooling curves from the melt (270°C), an exothermic crystallization peak (T_c) was observed, as shown in Figure 4. With increasing clay concentration, the position of T_c gradually shifted toward a higher temperature, whereas its magnitude decreased steadily (as shown in the insert in Fig. 4). This indicated that the added clay acted as effective nucleation sites,

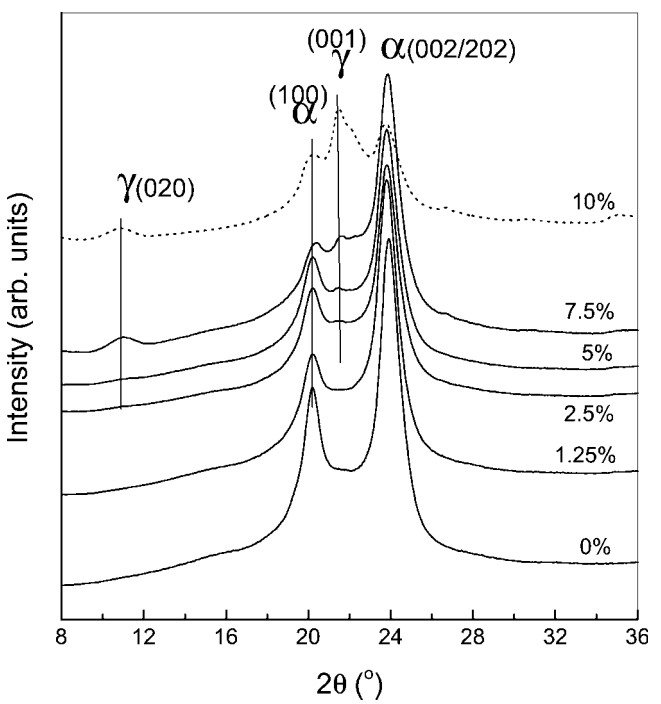

Figure 5 WAXD patterns of neat PA6 and the nanocomposite samples as a function of clay concentration.

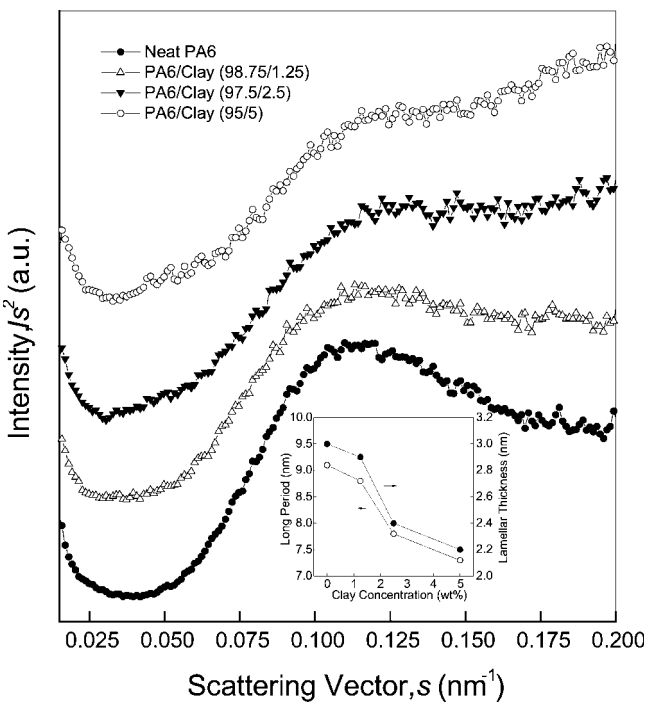

Figure 7 SAXS plots of Is^2 versus **s.** The insert shows the variation of L and l_c as a function of clay content.

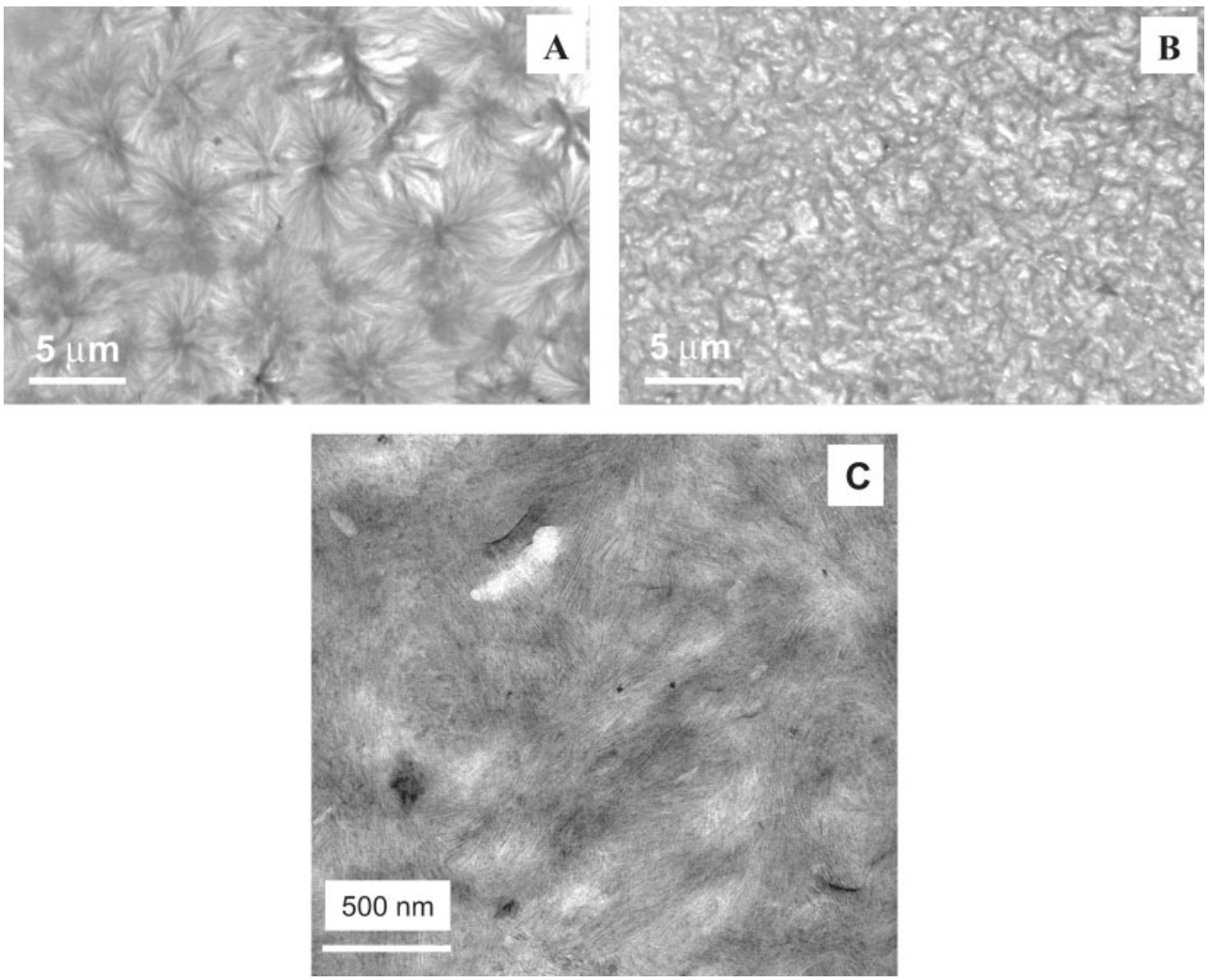

Figure 8 TEM morphological observations of (A) neat PA6 and (B) the nanocomposite sample with 2.5 wt % clay, and (C) the nanocomposite sample with 2.5 wt % clay under high magnification and stained with OsO_4.

which, however, significantly deteriorated the perfection of the crystalline structure.

The WAXD patterns as a function of clay loading are shown in Figure 5. The following structural features were seen:

1. For neat PA6, two main diffraction peaks were observed at about $2\theta = 20$ and 23.7°, which were attributed to the $\alpha(100)$ and $\alpha(002/202)$ crystal planes, respectively.[19,24–26] The α-form population was, therefore, the dominant crystalline phase in neat PA6.
2. In contrast, in addition to the two main diffraction peaks in neat PA6, another two peaks were observed at around $2\theta = 10.7$ and 21.4° for the PA6/clay nanocomposites. The latter two were associated with the $\gamma(020)$ and $\gamma(001)$ crystal planes of PA6, respectively.[19,24–26] Hence, the addition of clay induced the formation of γ-form crystals, which suggested a heterogeneous nucleation mechanism for the γ-form crystal formation.

Moreover, with increasing clay content, the intensity of the $\alpha(100)$ peak (at $2\theta = 20^\circ$) gradually decreased, which indicated that an $\alpha \rightarrow \gamma$ crystal transformation occurred on the addition of clay into the PA6 matrix, which was also confirmed by the DSC results shown in Figure 3.

Figure 6 shows the effect of concentration of the added clay on the crystallinity of the PA6 nanocomposites. The degrees of crystallinity ($W_{c,XRD}$ and $W_{c,DSC}$) were calculated based on the WAXD (Fig. 5) and DSC (Fig. 3) results, respectively. Despite the difference in the absolute values obtained by the WAXD and DSC methods, both $W_{c,XRD}$ and $W_{c,DSC}$ decreased by about 30% with increasing clay loading up to 10 wt %. Therefore, we concluded that the addition of nanoclay significantly reduced W_c of the PA6 matrix, as also

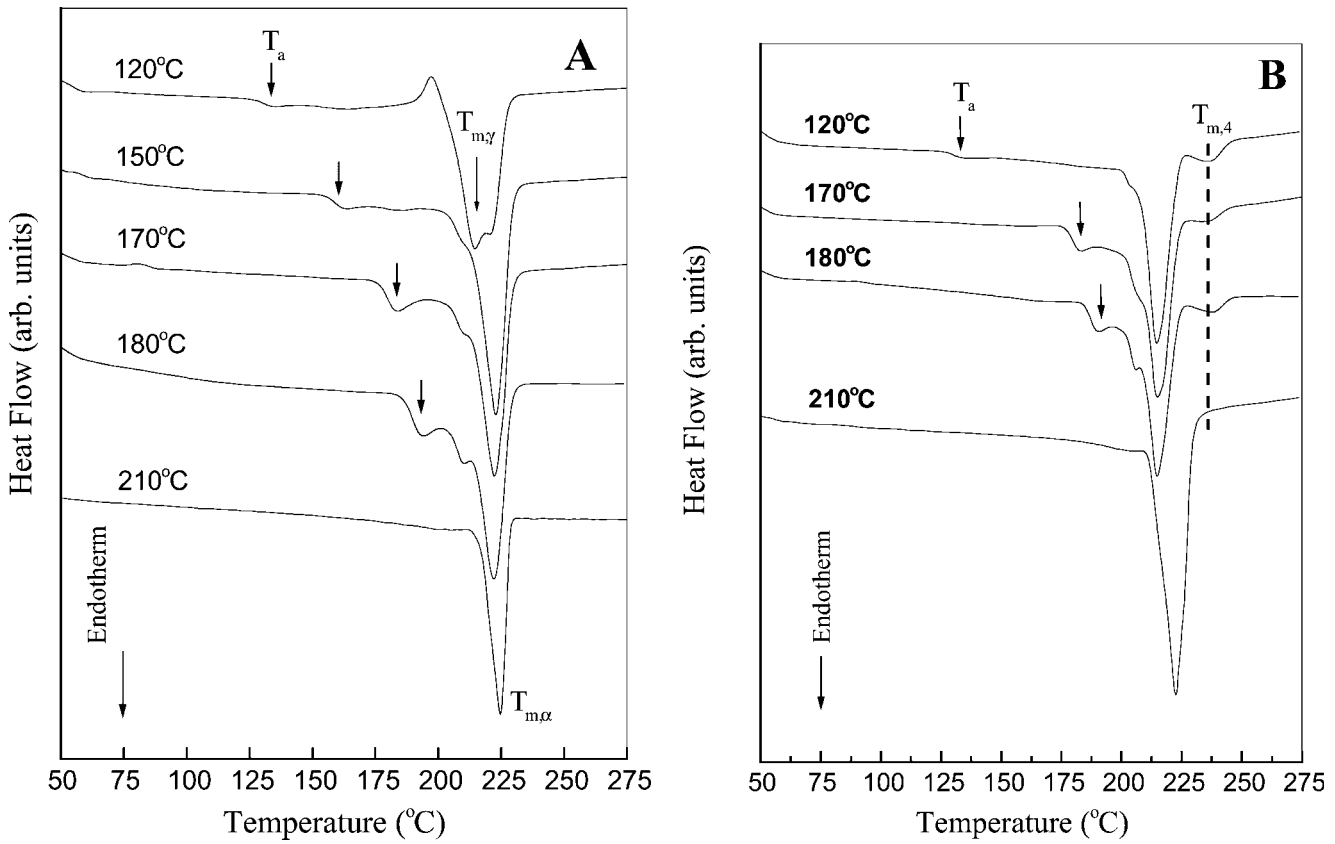

Figure 9 DSC heating curves for (A) neat PA6 and (B) the nanocomposite sample (with 5 wt % clay) annealed at the indicated temperatures (heating rate = 10°C/min).

previously observed in nylon 66 nanocomposites.[31,32] Such dramatic changes in the microstructure (i.e., the reduced crystallinity) with increasing clay content have been suggested to be attributable to the deterioration of creep resistance of the materials, especially at higher clay loadings.[33] The two competing factors (i.e., the reinforcement from rigid nanoclay and the degeneration of crystalline structure) simultaneously affect the creep behavior of the nanocomposites. Detailed investigations of the changes in crystalline morphologies on the mechanical properties by nanoindentation were reported separately.[33]

Morphological observations by SAXS and TEM

The changes in the crystalline morphologies of the PA6 matrix due to addition of clay were investigated by SAXS and TEM. Figure 7 illustrates $I\mathbf{s}^2$ versus scattering vector ($\mathbf{s}$) curves (where I is the scattering intensity and $\mathbf{s} = 2 \sin \theta/\lambda$) from the SAXS measurements for neat PA6 and the nanocomposites as a function of clay content. As shown in the insert in Figure 7, L and l_c decreased significantly with increasing loading of the clay nanofiller, as observed by other researchers in the same system.[12,34,35]

Figure 8(A) shows the TEM image of a thin section of neat PA6 (microtomed from the extruded pellet sample followed by OsO_4 staining). A number of typical crystalline spherulites were observed with a size of about 5 μm. The well-developed spherulites consisted of numerous closely stacked fibrillar lamellae, which radially grew outward from the central regions (i.e., the nuclei). With the incorporation of nanoclay (e.g., 2.5 wt %) into the PA6 matrix, however, the crystalline texture of the matrix was severely obscured, as shown in Figure 8(B). The crystal size decreased dramatically, and the well-defined spherulites were absent, probably due to the high (heterogeneous) nucleation density from clay nanofiller; only numerous bundlelike dark regions were observed with certain contrast. At higher magnification [Fig. 8(C)], these blurred crystalline bundles were seen; they consisted of closely packed lamellae. Close inspection also showed the presence of nanoclay platelets (the darkest lines or regions).

Thermal behavior of PA6 and its nanocomposites as studied by DSC

As discussed previously, the addition of clay into PA6 matrix significantly changed the crystallization behavior of the polymer matrix. Accordingly, this was reflected from the thermal behavior of the nanocomposites. In this section, the thermal behavior of the

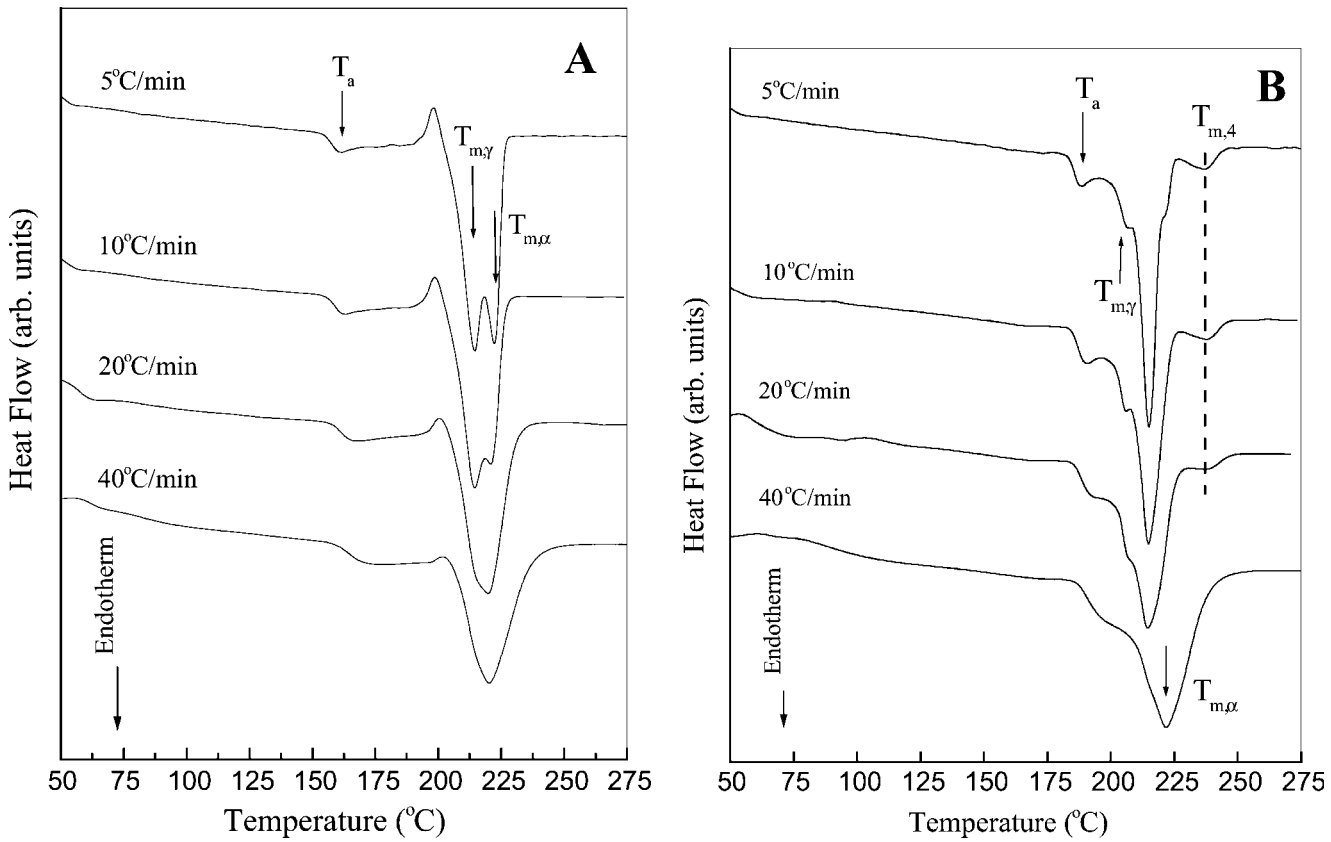

Figure 10 DSC heating curves for (A) neat PA6 and (B) the nanocomposite sample (with 5 wt % clay) scanned at various heating rates as indicated.

nanocomposites is discussed and compared with that of neat PA6, as studied by DSC.

Figure 9(A,B) illustrate the effect of T on the thermal behavior of neat PA6 and the nanocomposite (with 5 wt % clay, as an example) samples (which were melt-crystallized at the indicated temperatures for 6 h):

1. In the main melting region of PA6 and the nanocomposite, the positions of $T_{m,\gamma}$ and $T_{m,\alpha}$ were relatively constant with increasing T. It seemed that the formation of γ crystals was preferred at low temperatures (e.g., 120°C), whereas the α-form population was dominant at higher temperatures [see Fig. 9(A)].
2. For PA6, an exothermic peak at about 195°C was observed for $T = 120$°C; this probably indicated that some uncrystallized materials may have underwent reorganization or recrystallization during the heating process. Such a recrystallization process was significantly suppressed at higher T's for neat PA6 and was not pronounced for the nanocomposite system [Fig. 9(B)].
3. Another endothermic peak (indicated by arrows), the so-called annealing peak (T_a), was induced by the isothermal crystallization or annealing process for both PA6 and the nanocomposite systems. The T_a peak increased in magnitude and shifted toward higher temperatures (always about 10°C above T) as T increased. This annealing-induced endotherm is a universal phenomenon in most semicrystalline thermoplastic polymers, including poly(aryl ether ketone), poly(phenylene sulfide), poly(ethylene terephthalate),[36] and isotactic polystyrene.[37–39] The physical origins of this behavior are still under debate in the literature. In our previous report, we tentatively ascribed it to an enthalpic relaxation process of the interphase between the crystalline and amorphous phases.[37–39] Some preliminary dynamic mechanical analysis and modulated DSC results on PA6 and the nanocomposites also support this speculation with the observation of an extra glass transition at about 10°C above T.[40] A more detailed study on the T_a will be presented in a separate report.
4. At an even higher T's (e.g., $T = 210$°C), all the melting peaks merged into one at about 220°C. The abnormal $T_{m,4}$ (indicated by the dashed line) was probably overlapped at such high temperatures for the nanocomposite [Fig. 9(B)].

The effect of heating rate on the thermal behavior of PA6 and the nanocomposite is shown in Figure 10(A,B). With increasing heating rate, (1) the endo-

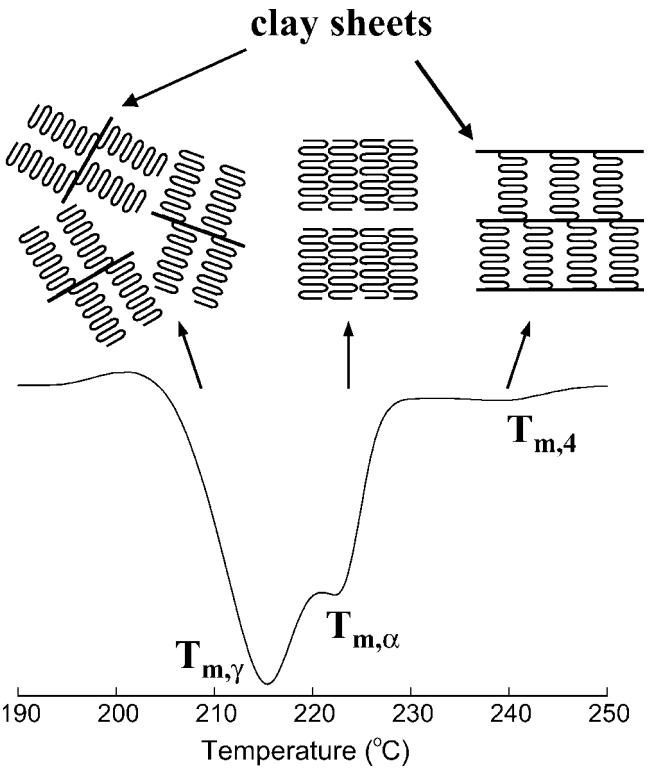

Figure 11 Schematic model of the possible origins of the multiple melting peaks observed in the DSC study of the nanocomposite samples.

thermic peak T_a slightly shifts toward higher temperatures due to thermal lag, (2) the recrystallization (ca. 200°C) was suppressed because less time was available, and (3) the double melting peaks of the γ-form and α-form crystals ($T_{m,\gamma}$ and $T_{m,\alpha}$, respectively) eventually merged into a broad peak at about 224°C.

Compared to PA6, the most noticeable difference in the DSC curves for the nanocomposite was the appearance of the new endothermic peak ($T_{m,4}$) at around 237°C [see Figs. 3, 9(B), and 10(B)]. Such an abnormal endothermic peak was evidently closely related to the addition of clay into the polymer matrix, yet so far, the exact origins of this new peak are still unknown. This peak could not be attributed to organoclay itself because no thermal transitions were observed around this region from the DSC curves of clay (not shown here). It could not be ascribed to an organoclay-induced new ordered or crystalline structure either because in the room-temperature and high-temperature WAXD patterns (not shown here), no new crystalline structure was identified. We speculated that this peak was due to the reorganization of the polymer matrix during the heating process; however, the DSC curves as a function of heating rate [see Fig. 10(B)] showed no convincing evidence because it was difficult to deconvolute the $T_{m,4}$ peak because of its proximity to $T_{m,\alpha}$.

This new melting peak ($T_{m,4}$) around 237°C reminded us of some other research work on layered silicate/polymer nanocomposites. Most recently, it has been documented that the statics and dynamics of polymers within the host galleries are dramatically different from those observed in the bulk, due not only to the confinement of the polymer chains but also to specific polymer–surface interaction, normally not observed in the bulk.[1,41,42] Furthermore, one of the most striking results (on layered silicate/polyamide 12 nanocomposites) from TEM morphological observation by Kim et al.[43] directly showed that the fine lamellae of polyamide 12 were oriented with their planes perpendicular to the injection-molding direction because of nucleation at the interface between layered silicate and polymer matrix. Interestingly, the orientation of the polymer (PA6) lamellae relative to the organoclay sheets was also confirmed to be orthogonal by SAXS.[30] Thus, we expect that the intercalated nanoclay sheets imposed stresses on the PA6 lamellae, which were tethered on the host layers by strong (interfacial) ionic interaction. As a result, a superheating effect may have resulted as these constrained lamellae within the confined environment were heated in DSC. Therefore, we attributed this abnormal endothermic peak to the melting of PA6 lamellae formed in the microenvironments of nanoclay platelets in the intercalated nanocomposites. A preliminary result supported our argument: in comparison to the case in highly confined intercalated systems, such an abnormal melting peak in the polymer matrix on exfoliation of the organoclay became much weaker or even disappeared.[40]

To summarize, a schematic model was proposed to explain the complex melting behavior observed (Fig. 11). On the one hand, the addition of clay into the PA6 matrix induced more nucleation sites and facilitated the formation of γ-phase crystals. Thus, the less stable γ crystals were melted at low temperatures (i.e., $T_{m,\gamma}$) during heating. On the other hand, the stable crystals (i.e., α phase) freely formed from polymer chains melted at high temperatures (i.e., $T_{m,\alpha}$). Finally, the constrained crystals formed within the confined environment of the (intercalated) clay galleries were melted at even higher temperatures (i.e., $T_{m,4}$) because of the superheating effect.

CONCLUSIONS

The nanostructure and morphology of the PA6/clay nanocomposites as a function of clay loading were systematically investigated by means of WAXD, TEM, DSC, and SAXS. The combination of WAXD and TEM data illustrated an exfoliated clay morphology within the PA6 matrix. The DSC and WAXD results show an evident phase transformation from α-form to γ-form

crystals, which indicate that the introduction of nanoclay fillers into the polymer matrix had a strong heterophase nucleation effect, which was favorable for the formation of the less stable γ-form crystals of PA6. TEM and SAXS results indicate, respectively, that with increasing clay concentration, the spherulitic morphology of PA6 was significantly obscured and the crystallinity, l_c, and L of PA6 decreased dramatically. DSC results reveal a new high melting transition around 237°C for the nanocomposites, which was probably due to the crystallization of polymer chains under a confined environment. A model was proposed to explain this multiple melting behavior of the nanocomposites.

References

1. Giannelis, E. P.; Krishnamoorti, R.; Manias, E. Adv Polym Sci 1999, 138, 107.
2. Kojima, Y.; Usuki, A.; Kawasumi, M.; Okada, A.; Fukushima, Y.; Kurauchi, T.; Kamigaito, O. J Mater Res 1993, 8, 1185.
3. Cho, J. W.; Paul, D. R. Polymer 2001, 42, 1083.
4. Fu, X.; Qutubuddin, S. Polymer 2001, 42, 807.
5. Kojima, Y.; Usuki, A.; Kawasumi, M.; Okada, A.; Kurauchi, T.; Kamigaito, O. J Polym Sci Part A: Polym Chem 1993, 31, 983.
6. Usuki, A.; Kawasumi, M.; Kojima, Y.; Okada, A.; Kurauchi, T.; Kamigaito, O. J Mater Res 1993, 8, 1174.
7. Usuki, A.; Kojima, Y.; Kawasumi, M.; Okada, A.; Fukushima, Y.; Kurauchi, T.; Kamigaito, O. J Mater Res 1993, 8, 1179.
8. Fornes, T. D.; Yoon, P. J.; Keskkula, H.; Paul, D. R. Polymer 2001, 42, 9929.
9. Fornes, T. D.; Yoon, P. J.; Hunter, D. L.; Keskkula, H.; Paul, D. R. Polymer 2002, 43, 5915.
10. Lincoln, D. M.; Vaia, R. A.; Wang, Z. G.; Hsiao, B. S. Polymer 2001, 42, 1621.
11. Medellin-Rodriguez, F. J.; Burger, C.; Hsiao, B. S.; Chu, B.; Vaia, R. A.; Phillips, S. Polymer 2001, 42, 9015.
12. Lincoln, D. M.; Vaia, R. A.; Wang, Z. G.; Hsiao, B. S.; Krishnamoorti, R. Polymer 2001, 42, 9975.
13. Liu, X.; Wu, Q. Eur Polym J 2002, 38, 1383.
14. Liu, X.; Wu, Q. Polymer 2002, 43, 1933.
15. Dabrowski, F.; Bourbigot, S.; Delobel, R.; Le Bras, M. Eur Polym J 2000, 36, 273.
16. Krishnamoorti, R.; Yurekli, K. Curr Opin Colloid Interface Sci 2001, 6, 464.
17. Liu, L. M.; Qi, Z. N.; Zhu, X. G. J Appl Polym Sci 1999, 71, 1133.
18. Mathias, L. J.; Davis, R. D.; Jarrett, W. L. Macromolecules 1999, 32, 7958.
19. Wu, T. M.; Liao, C. S. Macromol Chem Phys 2000, 201, 2820.
20. Liu, T. X.; Mo, Z. S.; Zhang, H. F.; Li, G. J Appl Polym Sci 1998, 69, 1829.
21. Strobl, G. R.; Schneider, M. J. J Polym Sci Polym Phys 1980, 18, 1343.
22. Strobl, G. R.; Schneider, M. J.; Voigt-Martin, I. G. J Polym Sci Polym Phys 1980, 18, 1361.
23. Liu, T. X.; Tjiu, W. C.; He, C. B.; Na, S. S.; Chung, T. S. Polym Int 2004, 53, 392.
24. Samon, J. M.; Schultz, J. M.; Wu, J.; Hsiao, B. S.; Yeh, F.; Kolb, R. J Polym Sci Part B: Polym Phys 1999, 37, 1277.
25. Schultz, J. M.; Hsiao, B. S.; Samon, J. M. Polymer 2000, 41, 8887.
26. Ramesh, C.; Bhoje Gowd, E. Macromolecules 2001, 34, 3308.
27. Alexandre, M.; Dubois, P. Mater Sci Eng Rep 2000, 28, 1.
28. Kojima, Y.; Usuki, A.; Kawasumi, M.; Okada, A.; Kurauchi, T.; Kamigaito. O. J Polym Sci Part A: Polym Chem 1993, 31, 1755.
29. Kickelbick, G. Prog Polym Sci 2003, 28, 83.
30. Varlot, K.; Reynaud, E.; Kloppfer, M. H.; Vigier, G.; Varlet, J. J Polym Sci Part B: Polym Phys 2001, 39, 1360.
31. Shen, L.; Phang, I. Y.; Chen, L.; Liu, T. X.; Zeng, K. Y. Polymer 2004, 45, 3341.
32. Shen, L.; Phang, I. Y.; Liu, T. X.; Zeng, K. Y. Polymer 2004, 45, 8221.
33. Shen, L.; Tjiu, W. C.; Liu, T. X. Polymer 2005, 46, 11969.
34. Lincoln, D. M.; Vaia, R. A.; Krishnamoorti, R. Macromolecules 2004, 37, 4554.
35. Fornes, T. D.; Paul, D. R. Polymer 2003, 44, 3945.
36. Bonnet, M.; Rogausch, K.-D.; Petermann, J. Colloid Polym Sci 1999, 277, 513.
37. Liu, T. X.; Yan, S. K.; Bonnet, M.; Lieberwirth, I.; Rogausch, K.-D.; Petermann, J. J Mater Sci 2000, 35, 5047.
38. Liu, T. X.; Petermann, J. Polymer 2001, 42, 6453.
39. Liu, T. X. Eur Polym J 2003, 39, 1311.
40. Liu, T. X. Fudan University, unpublished results.
41. Vaia, R. A.; Giannelis, E. P. Macromolecules 1997, 30, 7990.
42. Vaia, R. A.; Giannelis, E. P. Macromolecules 1997, 30, 8000.
43. Kim, G. M.; Lee, D. H.; Hoffmann, B.; Kressler, J.; Stoeppelmann, G. Polymer 2001, 42, 1095.